Exploratory Study of Ovarian Intraepithelial Neoplasia

Molly A. Brewer,[1] James Ranger-Moore,[2] Amy Baruche,[3] David S. Alberts,[4] Mark Greene,[5] Deborah Thompson,[6] Yun Liu,[7] John Davis,[3] and Peter H. Bartels[6]

[1]Department of Obstetrics and Gynecology, Division of Gynecologic Oncology, [2]Division of Epidemiology and Biostatistics, [3]Departments of Pathology, [4]Medicine, Pharmacology, and Public Health, [5]National Cancer Institute, and [6]Optical Sciences Center, [7]Arizona Cancer Center, University of Arizona, Tucson, Arizona

Abstract

Purpose: **This was an exploratory study to test two hypotheses related to potential epithelial precursors to ovarian cancer: (*a*) histologically normal ovarian surface epithelium exhibited changes in the nuclear chromatin pattern, which indicate an ovarian abnormality, and (*b*) such changes were detectable in the ovarian surface epithelium of cancer-free subjects who were at high risk for ovarian cancer.**

Experimental Design: **Ovaries were carefully collected to avoid damage to the surface epithelium. Five-micron-thick histologic sections were cut and stained with H&E. High-resolution images were recorded from the ovarian surface epithelium and from the underlying stroma of ovaries from normal women (10 cases), women at high risk of developing ovarian cancer (7 cases), and histologically normal areas adjacent to ovarian cancer (3 cases). Karyometric features and measurements of nuclear abnormality were computed for 3,390 epithelial nuclei. Discriminant function analyses and unsupervised learning algorithms were employed to define deviations from normal and to identify the subpopulations of nuclei exhibiting these changes.**

Results: **Epithelium from ovaries harboring a malignant lesion had changes in the nuclear chromatin pattern consistent with a second phenotype, which were not visually detected with histopathologic surveillance. This phenotype was also present in the ovaries obtained from women at increased risk of ovarian cancer, suggesting that it may represent a premalignant abnormality. These changes were statistically significant.**

Conclusion: **The observed changes in karyometric features were sufficiently distinct to warrant further study as both diagnostic and prognostic biomarkers for early detection and prevention of ovarian cancer.** (Cancer Epidemiol Biomarkers Prev 2005;14(2):299–305)

Introduction

Ovarian cancer has the highest mortality of all gynecologic cancers; 70% of women with ovarian cancer die of their disease within 5 years. Although major progress has been made toward increasing the disease-free interval for women with ovarian cancer, there has been little impact on 5-year survival. Survival is high in women who present with early stage disease, but the lack of specific symptoms, the relative inaccessibility of the ovaries deep in the pelvis, and the absence of information about precursor lesions represent barriers to early detection. The treatment of stage III or stage IV ovarian cancer is highly morbid, expensive, and associated with high recurrence and mortality rates. Although the overall cumulative lifetime risk of ovarian cancer is relatively low (1.5-1.7%; ref. 1), there are subgroups of women with moderately or significantly increased risks of ovarian cancer who have a higher disease prevalence. Women with a family history suggestive of hereditary breast/ovarian cancer syndrome are at exceedingly high risk with lifetime risk of developing ovarian cancer ranging from 16% to 40% (2). Such women would benefit greatly from effective early detection methods, which currently do not exist.

One of the challenges related to early detection and prevention of ovarian cancer has been the uncertainty as to whether a premalignant or precursor lesion exists (3-9). In other organ systems, such lesions have been critical to the success of early detection programs (e.g., cervical intraepithelial neoplasia for carcinoma of the uterine cervix, ductal carcinoma *in situ* for breast cancer, and advanced adenomatous polyps in colorectal cancer). These abnormalities can be identified and treated in the early stages of carcinogenesis, which prevents the development of invasive cancer. At the present time, this cannot be accomplished for ovarian cancer. Small collections of malignant cells contiguous with normal ovarian epithelium suggestive of an intraepithelial neoplasia, but not involving underlying tissues, can be found in ovaries removed from women who eventually develop primary peritoneal carcinomatosis (5), high-risk women who undergo prophylactic oophorectomy (5, 6), and in areas adjacent to stage I cancers that show a transition from malignant to normal epithelium (7). However, a characteristic histologic precursor lesion for ovarian cancer is not apparent in all prophylactic oophorectomy specimens (8, 9). Nonetheless, women at increased genetic risk of ovarian cancer are sufficiently motivated to undergo periodic screening with transvaginal ultrasound and CA125 measurements or, recognizing that there is little evidence of benefit associated with screening strategies, may consider risk-reducing salpingo-oophorectomy. However, prophylactic oophorectomy in young women is complicated by the morbidity due to premature menopause and concerns regarding the possible risks of hormones in a setting which includes a slightly increased risk of breast cancer (10).

The techniques of computerized image analysis of cells have been refined to allow the detection of very subtle changes in nuclei which are associated with evolving preneoplastic lesions in a number of tissues (11, 12). The detection of abnormal nuclear characteristics related to changes in the organization of nuclear chromatin may identify subpopulations of cells in which studies of gene and/or protein expression might elucidate mechanisms of ovarian carcinogenesis. Such knowledge could bring considerable insight into the pathogenesis of ovarian cancer. The long-range goals of applying these imaging techniques to the study of ovarian cancer are (*a*) to determine if this methodology has the potential for use as a screening tool

Received 3/17/04; revised 9/9/04; accepted 9/29/04.

Grant support: NIH National Cancer Institute grant CA 53877-13 (P.H. Bartels).

The costs of publication of this article were defrayed in part by the payment of page charges. This article must therefore be hereby marked advertisement in accordance with 18 U.S.C. Section 1734 solely to indicate this fact.

Note: The contents are solely the responsibility of the authors and do not necessarily represent the official view of the National Cancer Institute.

Requests for reprints: Molly A. Brewer, Department of Obstetrics and Gynecology, Division of Gynecologic Oncology, Arizona Cancer Center, Room 1968G, 1515 North Campbell Avenue, Tucson, AZ 85724-5024. Phone: 520 626-9283; Fax: 520 626-9287. E-mail: mbrewer@azcc.arizona.edu

in women at increased genetic risk of ovarian cancer, (*b*) to determine if surface epithelial cells can be evaluated successfully for nuclear chromatin changes that are linked to carcinogenesis, and (*c*) to identify premalignant changes in the ovary, which might serve as an intermediate end point in assessing new chemoprevention or screening strategies for ovarian cancer. This exploratory study was undertaken to test the hypothesis that histologically normal-appearing ovarian epithelium from cases harboring an ovarian lesion exhibits so-called malignancy-associated changes characterizing preneoplastic lesions which cannot be perceived by standard light microscopy but which are computationally detectable through karyometric analysis.

Materials and Methods

Patient Selection. The ''normal risk'' group was comprised of women undergoing incidental oophorectomy for benign indications and who lacked a familial predisposition to ovarian cancer (1.4-1.7% estimated lifetime risk). The ''high-risk'' group was comprised of women with a family or personal history of breast and/or ovarian cancer, which implies a higher risk of developing ovarian cancer (>5% lifetime risk) as evaluated by a board certified genetic counselor after review of all pathology reports that were accessible (95%) to document the presence of related cancers. Risk was assessed with the BRCA-PRO which uses the Berry-Parmigiani method of risk assessment (13). This group includes a small percentage of patients who will have undergone genetic testing for *BRCA-1* and *BRCA-2* through Myriad Genetics; those that carry a germ-line mutation will have a much higher probability of developing ovarian cancer than other patients (*BRCA-1*, 40-60% lifetime risk; *BRCA-2*, 8-10% lifetime risk). Patients were consented using a University of Arizona Institutional Review Board–approved consent form. Ovaries were harvested at the time of laparoscopic or open oophorectomy and were minimally handled intraoperatively and at the pathology bench to avoid denuding the surface epithelium.

Clinical Site of Selection and Acquisition. All slides were reviewed by a single gynecologic pathologist (J.D.) and cells selected were determined to be normal. The following dyads are used to denote the data sets. All nuclei were measured in histologically normal-appearing epithelium following expert pathology review. This is denoted by the first term ''norm.'' The term following a slash indicates that the ovarian tissue originated from normal-appearing ovarian tissue from a normal risk subject (norm/norm), normal-appearing ovarian tissue from a high-risk subject (norm/HR), or normal-appearing ovarian tissue from a woman with ovarian cancer (norm/Ca). Later, subpopulations were formed based on a threshold set in a discriminant function score distribution. These subpopulations were identified by the letter ''b'' for below threshold or ''a'' for above threshold (e.g., norm/HR a versus norm/HR b). The pathology materials for this pilot study consisted of H&E-stained histopathologic sections of histologically normal-appearing ovarian epithelium from 10 low-risk women, with 1,590 nuclei measured (norm/norm); from 7 women who were considered at high risk of ovarian cancer, with 1,300 nuclei measured (norm/HR); and from 3 women with an adjacent ovarian cancer, in which 500 nuclei in the histologically normal-appearing epithelium were analyzed (norm/Ca). Figure 1A-C illustrates a typical high-power, H&E-stained, light microscopy field for each of the three diagnostic categories. All are considered histologically normal by standard pathology criteria.

Data Acquisition and Analysis Procedures. The recording was done with a 100:1 planapochromatic oil immersion objective, numerical aperture 1.40 (Zeiss, Oberkochen). The relay optics adjusted image sampling to 6 pixels per micron. Image recording was done with a Sony DXC9000, 3CCD color camera (Sony Corporation, Melville, NY). For maximum contrast in the H&E stained sections, only the red channel image was used for feature computation.

After image segmentation, a set of 93 karyometric features was computed for each nucleus. These provided numerical values for the global features: nuclear area, total absorbance, and variance of pixel absorbance values (3 features); a relative frequency histogram of pixel absorbance values at 0.10 absorbance interval (18 features); the upper diagonal of the co-occurrence matrix of pixel absorbance values, 6 absorbance intervals each 0.30 absorbance unit wide (21 features); a matrix of run length features 6 absorbance intervals 0.30 absorbance unit wide versus six run length intervals from 1 to 12 pixels (36 features); and a number of summarizing features of the chromatin texture, such as run length emphasis, mean pixel absorbance, and histogram shape (15 features; refs. 13, 14).

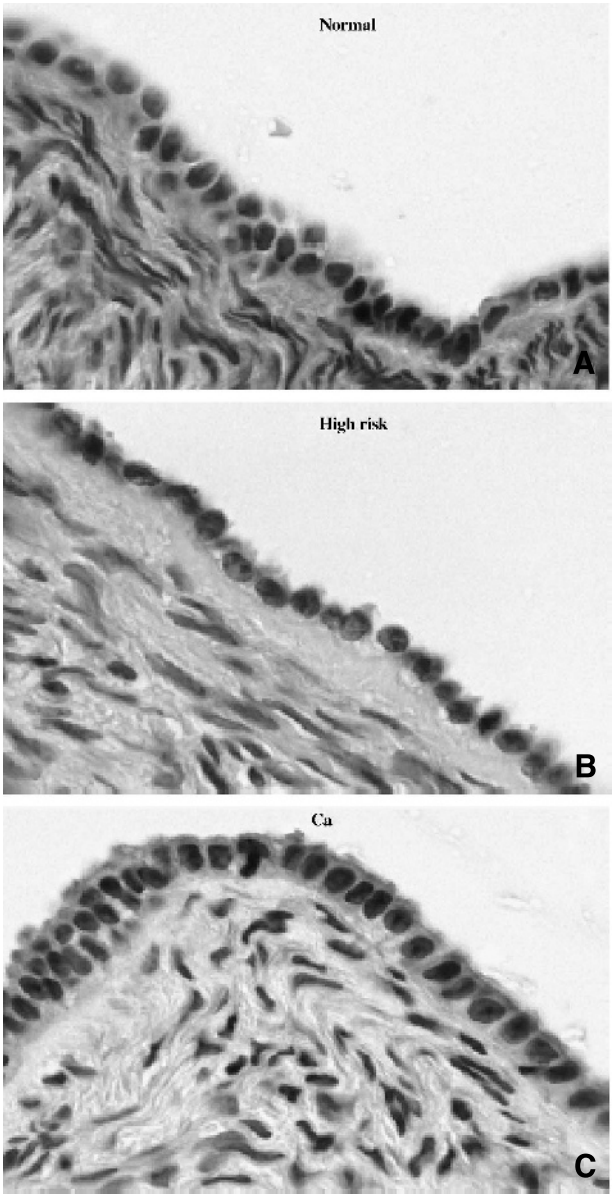

Figure 1. Representative images of the ovarian epithelium from the norm/norm, norm/HR, and norm/Ca cases.

Table 1. Feature values for norm/norm and norm/Ca diagnostic categories

	norm/norm (CI)	norm/Ca (CI)
Total absorbance	0.167 (0.16-0.17)	0.235 (0.23, 0.24)
Variance of pixel absorbance values	18.41 (18.19-18.63)	24.48 (23.99, 24.97)
Dn/n of pixels, 0.80-0.90 absorbance interval	2.98 (2.60, 3.36)	14.76 (13.51, 15.96)
Co-occurrence, interval 4 to 1	4.3 (3.64, 4.95)	24.23 (23.29, 25.17)
Run length uniformity	4.52 (4.45, 4.60)	6.77 (6.59, 6.96)
Average pixel absorbance 20% above mean absorbance	35.2 (34.88, 35.5)	50.5 (49.7, 51.3)

Abbreviation: CI, confidence interval.

Two numerical measures of deviation from normal were computed. First, the nuclear abnormality for each nucleus based on the nuclear signature (14, 15) and the distribution of nuclear abnormality values in a biopsy were computed. To form the nuclear signature, a reference set of nuclei from the norm/norm data set was used. For these nuclei, the mean and SD of each feature was computed. Thus, for each referenced nucleus, the absolute difference from the mean value of the corresponding reference feature was taken and divided by the corresponding SD for the reference feature. Thus, the deviation from normal is expressed as a ''standardized distance'' or z value. The nuclear signature is formed by arranging the z values for the 93 features in an arbitrary but consistent order as a bar graph.

It is also possible to form an average over the 93 z-values. The result is a single number that is referred to as ''nuclear abnormality.'' The distribution of nuclear abnormality values in a biopsy is called the lesion signature.

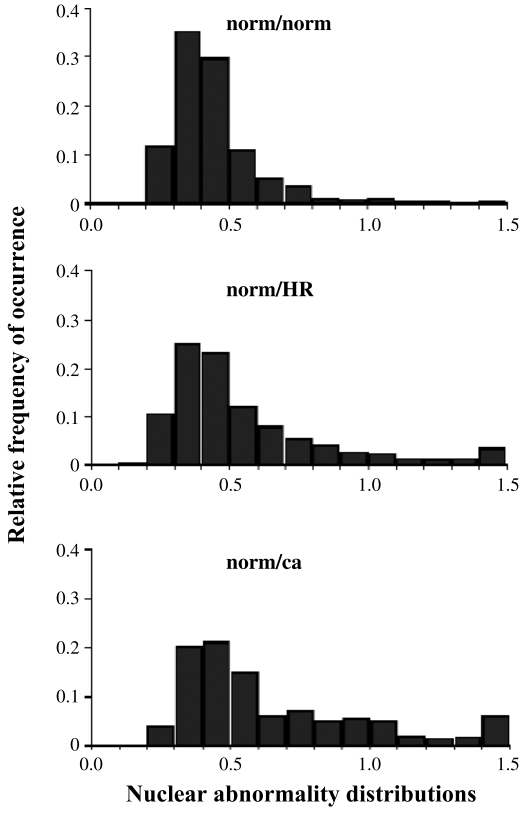

Figure 2. Lesion signatures for the three diagnostic categories for the surface epithelial nuclei.

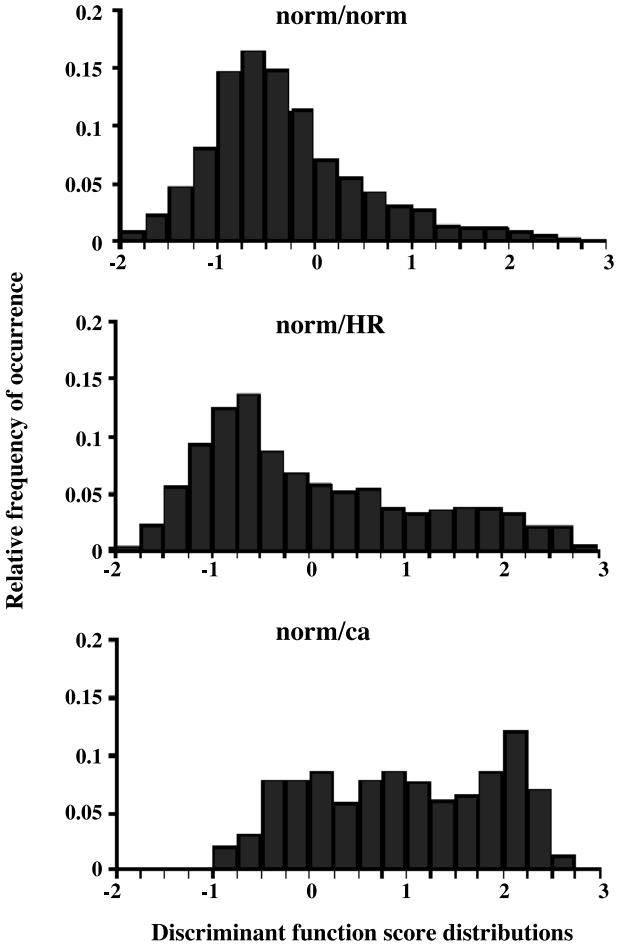

Figure 3. Score distributions for discriminant function I for the three diagnostic categories for surface epithelial nuclei.

The second numerical measure employed in this study consists of discriminant function scores. Discriminant function I was derived to separate surface epithelial nuclei in the norm/norm data set from those of the norm/Ca data set.

Results

Figure 1A-C shows a typical high power field for each of the three diagnostic categories. For each nuclei, 93 karyometric features, descriptive of the spatial and statistical distribution of the nuclear chromatin, were computed. The values averaged overall nuclei in the norm/norm diagnostic category, and norm/Ca shows an increase for a number of features (see Table 1). All feature values are given in arbitrary relative units.

The distribution of nuclear abnormality values (an average deviation from normal based on all 93 feature values) shown in Fig. 2 shows a clearly expressed shift to higher abnormality values, both in the nuclei from norm/Ca and in the nuclei from norm/HR. The right histogram bin represents nuclei of abnormality greater than or equal to 1.5 rather than an interval equal to those further left. Thus, the differences in distribution skewness are even greater than depicted.

As expected, in the norm/norm data set, the mode is seen in the low value range. In the norm/HR and the norm/Ca distributions, a moderate proportion of nuclei extend into a range of 1.0 to 1.5 SD from normal.

The nuclear abnormality is a rather robust measurement formed by averaging all 93 features. At the same time, it is

somewhat insensitive because not all features are likely to change across the different categories. A discriminant function analysis tends to detect specific features expressing change and is therefore much more sensitive.

Discriminant function I analysis was carried out for the norm/norm versus the norm/Ca data sets. The nonparametric Kruskal-Wallis test identified more than 20 features differing significantly at $P < 0.005$. Of these, the six features from different feature groups (as shown in Table 1) were entered. The correct classification rate for nuclei in this training set was 78.5% (i.e., even the tolerance limits showed only moderate overlap). Given the high significance level used in the feature selection, the sample size to dimensionality ratio of almost 100:1, and the fact that a definitive estimate of classification correctness was not the prime objective, no test data set was run. In any case, the chances for including any spurious feature at all were less than 3%. Figure 3 shows the distribution of discriminant function scores for the norm/norm, the norm/HR, and the norm/Ca data sets.

It is evident that a second mode at high discriminant function values develops; this occurs in the norm/HR data set. In the norm/Ca data set, the mode characterizing normal epithelial nuclei is shifted toward high scores (i.e., higher abnormality) with the higher value mode further increased.

If one wants to define the changes in nuclear chromatin distribution that characterize these developments, it is essential that the contributions from normal epithelial nuclei present in these epithelia be excluded. Figure 4 shows a threshold setting on the discriminant function score axis, such that most normal epithelial nuclei are below, and nuclei exhibiting changes are above. This leads to the defining of several subpopulations: (*a*) norm/norm b (below) to represent the most normal nuclei; (*b*) norm/norm a (above) to represent those nuclei exceeding the threshold; (*c*) norm/HR b (below) and norm/HR a (above) to characterize nuclei from high-risk cases; and (*d*) norm/Ca b and norm/Ca a for nuclei from ovarian cancer cases. One finds the following proportions of nuclei above threshold: (*a*) norm/norm constitutes 10.8% of all norm/norm; (*b*) norm/HR a is 25.4% of all norm/HR; and (*c*) norm/Ca a is 57.4% of all norm/Ca. These subpopulations, formed on the basis of the discriminant function score distributions, have markedly different nuclear abnormality distributions (as shown in Fig. 5).

The nuclear signatures also show a notable change in certain features (as shown in Fig. 6). These changes are somewhat greater in the norm/Ca data set than in the norm/HR data set, but they are strikingly similar. They are also very similar to the nuclear signatures seen in histologically normal tissue from prostates with prostatic intraepithelial neoplasia lesions (16) where only a moderate number of features exhibit notable changes.

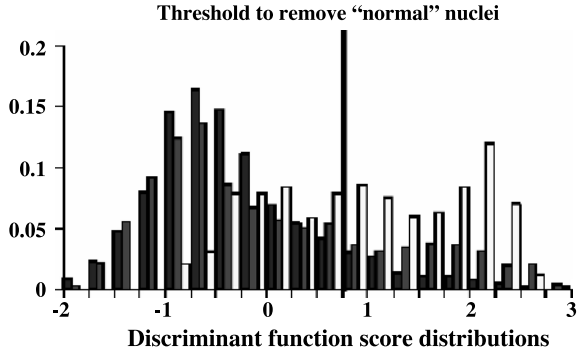

Figure 4. Threshold setting in the distribution of discriminant function scores to separate nuclei deviating from normal.

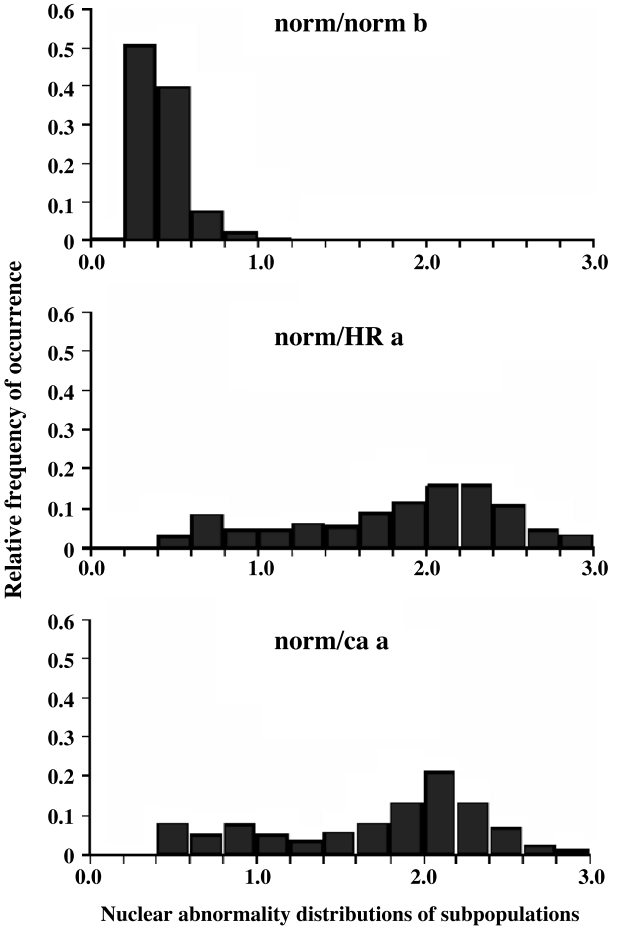

Figure 5. Distribution of nuclear abnormality for the surface epithelial nuclei from normal ovaries below the threshold from Fig. 4, for the surface epithelial nuclei from histologically normal ovaries from cases at high risk for ovarian cancer exhibiting signs of deviation form normal, and the same for histologically normal surface epithelial nuclei from cases of ovarian cancer.

Earlier studies have shown that features representing the forming of denser chromatin granules (as represented by the pixel absorbance histogram) are the first to undergo development of preneoplastic changes (17). In fact, the pixel absorbance histogram in the ovarian data set undergoes a steady shift towards higher pixel absorbance values in an almost identical fashion to the shift seen in one of the first karyometric studies, in the discrimination of tissue culture normal human embryonic lung cells versus human epidermoid carcinoma cells (18).

A plot showing the 95% confidence ellipses for the bivariate means for two nuclear texture features of the above-described subpopulations shows the monotonic rise from the still normal nuclei in norm/norm b and norm/HR b to the already changing nuclei in norm/Ca b in the norm/HR a and to norm/Ca a (as shown in Fig. 7). Two observations are noted: (*a*) In the norm/HR data set, the norm/HR b subpopulation is still the same as the norm/norm b nuclei. (*b*) However, this is no longer true for the norm/Ca b nuclei. This is seen in the average discriminant function scores for these subpopulations as shown in Table 2 below.

The results presented in Table 2 are a simplification, owing to the confidence intervals treating the nuclei as statistically independent. In reality, nuclei from the same individual are not independent. To account for this, we also conducted a mixed model analysis using SAS PROC MIXED, in which category was treated as a fixed effect and subjects were treated

as random. An exchangeable correlation structure was implemented. The statistical significance of inter-category differences mirrored those seen in Table 2.

In the norm/norm data set, a small percentage of nuclei (10.8 %) also exhibit feature values of the range expected in a population of normal epithelial nuclei (average discriminant function score of 1.783). As one would expect, whereas more abnormal than the nuclei below the threshold in all categories, they appear to be less abnormal than norm/HR a and norm/Ca a nuclei. In conclusion, normal epithelial cells from ovaries containing a malignant lesion do exhibit statistically significant differences in the values of features characterizing the nuclear chromatin pattern. They indicate the formation of denser granules of chromatin. Such a change is typical for chromatin in premalignant and malignant cells. Thus, the hypothesis is that in histologically normal ovarian epithelium, a field effect of preneoplastic ''malignancy associated changes'' can be seen at a high level of significance. In fact, not only are the mean feature values significantly different, the tolerance regions even show minimum overlap so that there is a prospect for diagnostic classification. To some extent, these changes are clearly expressed in a substantial proportion of nuclei from the ovarian epithelium of cases with no malignant lesions, but with a classification of high risk for development of ovarian cancer. Figure 8 shows a regression curve of the mean risk, which was calculated from the personal and family history of cancer, plotted against the discriminant function score. As risk increases, discriminant function score (i.e., nuclear abnormality) increases in a linear manner. Here, clearly a preneoplastic lesion is present.

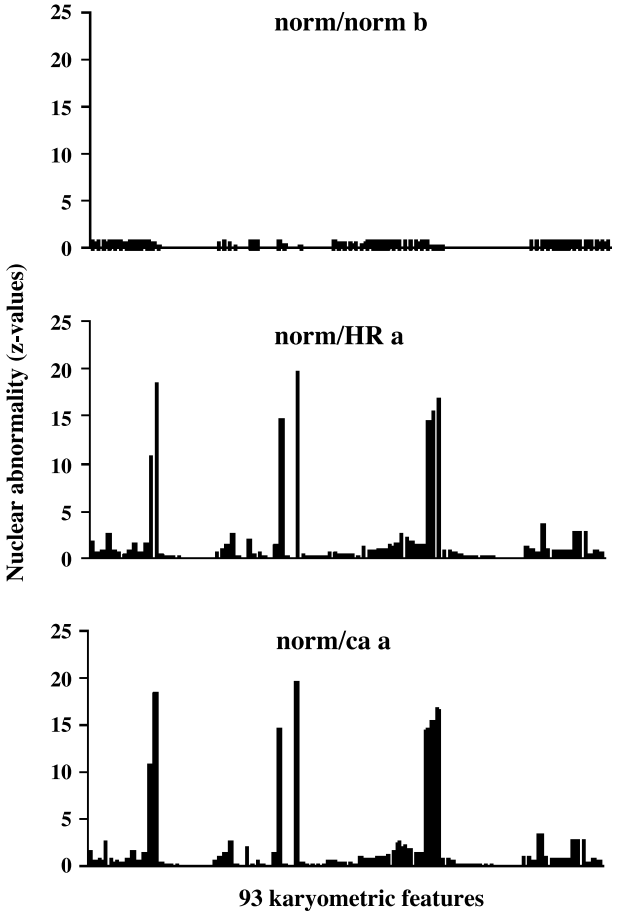

Figure 6. Nuclear signatures for the reference data set of normal epithelial nuclei and for the nuclei exhibiting signs of deviation from normal in the norm/HR and norm/Ca data sets.

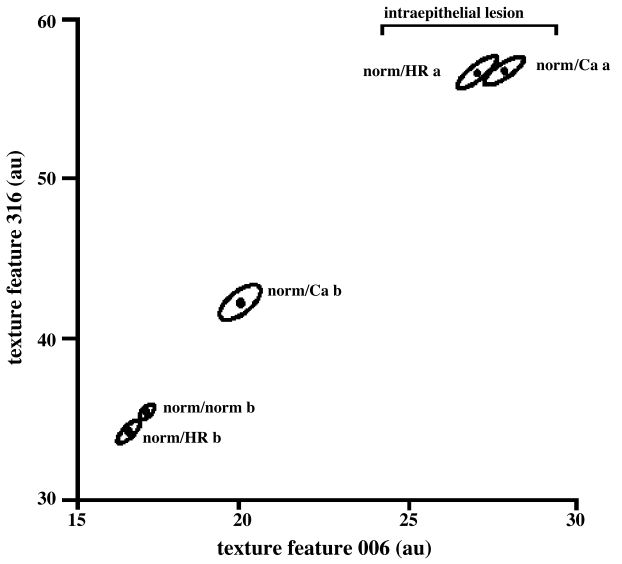

Figure 7. Bivariate plot showing the means and 95% confidence regions for two karyometric features, texture feature 006, the variance of pixel absorbance values, texture feature 316, and nuclear absorbance at a point 20% below the average value. The reference nuclei norm/norm b and the nuclei below threshold from the data set in high-risk cases are situated close together, but the nuclei below threshold for the cancer cases already appear changed in the direction of the mean values found for the nuclei clearly exhibiting deviation from normal in the high-risk and in the cancer cases. These represent changes in an intraepithelial lesion.

Power and Sample Size. This pilot data provides useful information in determining the sample size needed for subsequent studies. For simplicity, case averages of the average nuclear abnormality and discriminant function score were calculated and sample size determined on the basis of a simple t test. This is statistically conservative, in that each case provided one piece of information for each outcome, whereas in more extensive studies, mixed models that use the unique information contained in each nucleus would be implemented. The average nuclear abnormality ($\pm$ SD) was 0.438 $\pm$ 0.054 for normal women, 0.903 $\pm$ 0.628 for high-risk women, and 1.077 $\pm$ 0.703 for women with cancer. Based on a two-sided t test with a criterion probability of 0.05, a sample size of 20 women in each risk category would be required to achieve 80% power for a comparison of means between normal and high-risk women. As few as 13 women per each risk category would provide 80% power when comparing normal with cancer. It is possible to increase statistical power when comparing high-risk women with those with cancer by assessing the 10% worst nuclei only. As noted earlier, this approach reduces heterogeneity stemming from the fact that not all nuclei change for the worse across categories. For the 10% worst nuclei, the mean average nuclear abnormality was 1.593 $\pm$ 0.890 for high-risk women

Table 2. Average discriminant function scores for nuclei

Subpopulation	*N*	Score	CI
norm/norm b	2,293	−0.39	(−0.46, −0.38)
norm/HR b	875	−0.40	(−0.42, −0.38)
norm/Ca b	213	−0.22	(−0.27, −0.18)
norm/HR a	223	+2.06*	(1.94, 2.19)
norm/Ca a	287	+2.11*	(2.00, 2.22)

*The values for the latter two categories are given for comparison only.

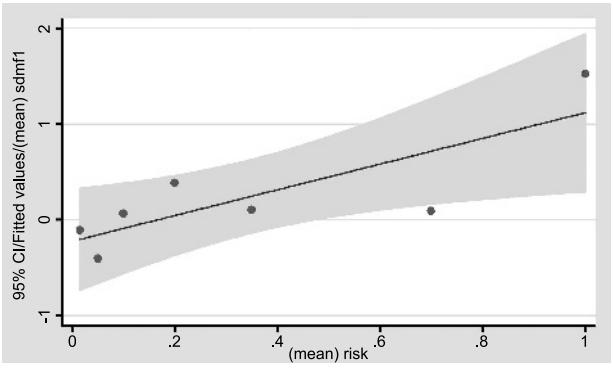

Figure 8. Regression curve for mean risk plotted against discriminant function values. There is a linear relationship between mean risk and karyometric abnormality.

and 2.445 ± 0.243 for women with cancer. In this analysis, ~13 women per risk group would provide 80% statistical power. The power analysis for discriminant function scores provides very similar numbers. Average discriminant function scores were −0.357 ± 0.118 for normal women, 0.496 ± 1.125 for high-risk women, and 0.945 ± 1.262 for women with cancer. For this outcome, 80% power can be achieved with sample sizes per risk group of 19 women, comparing normal with high-risk women; 10 women, comparing normal with women with cancer; and ~150 women, comparing high-risk with women with cancer. Again, an upper 10% threshold technique can be used, resulting in a mean discriminant function score of 1.334 ± 1.782 in high-risk women and 3.346 ± 0.265 in women with cancer. By focusing on only the most abnormal nucleus, 80% statistical power can be achieved with ~10 women per risk category.

The P-index algorithm (18), in its assessment of statistical significance of a difference between clusters, relies on the tolerance regions rather than on the difference in the cluster centroid location. The two clusters formed by the P-index were not found to be statistically significant, according to the Beale statistic ($P = 0.72$; ref. 19). However, when submitted to a Kruskal-Wallis test, the two clusters were shown to have statistically higher significant differences for more than 20 karyometric features at $P < 0.005$.

Discussion

This study was planned and executed as a pilot designed to explore the potential usefulness of nuclear karyometry in identifying epithelial ovarian changes which might be undetectable by standard light microscopy. The results show clearly the presence of changes in the nuclear chromatin in both the normal-appearing ovarian surface epithelium of the cases with ovarian cancer and the ovaries of women without an ovarian lesion but at increased risk for development of ovarian cancer, based on their personal or family history of breast and/or ovarian cancer. These abnormalities were present in the ovarian nuclei from women at normal risk of ovarian cancer, but in very small numbers. The recorded changes are similar to those observed in the histologically normal-appearing tissue of other organs harboring premalignant and/or malignant lesions [e.g. in the bladder (20), cervix (21), prostate (11), breast (22), colon (23), and thyroid (24)].

In the ovarian epithelium, the primary change is the development of chromatin granules that are optically denser than normal, leading to a shift in the pixel absorbance histogram towards higher absorbance values. Such a shift was first observed in one of the original analytic studies of digitized imaging of cells in cultured cells from human embryonic lung and from human epidermoid carcinoma (18). Shifts in the pixel absorbance histogram have been found to be one of the earliest indicators of change in the nuclear chromatin pattern (17). Such changes are seen not only in sections from ovaries harboring malignant lesions but also in the ovaries from women at increased risk of developing ovarian cancer who do not have a preneoplastic or neoplastic lesion. In these epithelia from higher risk women, a certain proportion of cells remained unchanged with the same characteristics as seen in the majority of the normal epithelium. This is no longer the case for the epithelium from ovaries harboring a malignant lesion. The entire ovarian surface epithelium seems to express a field defect in which there are few cells left with completely normal characteristics.

These changes in the chromatin pattern of nuclei in the histologically normal-appearing surface epithelium suggest the potential for the development of a malignant lesion or the presence of an already existing malignant lesion. One may call these tissue regions ''intraepithelial lesions'' or ''preneoplastic lesions,'' as clearly there is not yet any visually evident neoplasia. Our use of the term ''preneoplastic'' is meant to suggest that these changes are consistent with very early signs of the onset of a neoplastic process that is not yet apparent by visual inspection and, certainly, before any change in tissue architecture. In the literature, the term ''malignant associated change'' has been used, as these changes were first observed in cases with a co-occurring carcinoma. Since then, the nuclear chromatin changes have been seen associated with premalignant lesions. However, there is no conclusive evidence that the changes in the chromatin pattern herald an inevitable progression to malignancy. In fact, it is a common misconception that precursor lesions are destined or obligated to progress to invasive malignancy. Malignant transformation is a stepwise, stochastic process in which the transition from one stage to the next is a relatively uncommon event. The presence of a preneoplastic lesion signals an increase in the risk of malignant transformation but does not guarantee that such transformation will occur.

One of the limitations of this study is the composition of the high-risk group. All women in this group had an increased risk of ovarian cancer because of their personal or family history of breast or ovarian cancer. However, they were heterogeneous in the sense that their lifetime risk ranged from 5% to 40%. The majority of publications have designated the high-risk group as known carriers of a *BRCA-1* or *BRCA-2* mutation. Thus, our study is limited somewhat by this heterogeneity. However, the lack of heterogeneity would underemphasize the effects of risk on nuclear abnormalities.

In conclusion, we have provided novel evidence in support of the hypothesis that distinctive changes in the nuclear chromatin pattern can be detected in the histologically normal-appearing ovarian epithelium from women with or at high risk of developing ovarian cancer. This suggests that there may well be a recognizable precursor lesion related to ovarian cancer which has not been previously characterized, due to its lying below the limits of visual detection afforded by standard light microscopy. These provocative pilot data warrant confirmation in a larger, appropriately powered replication data set.

If our preliminary observations prove correct, the implications for the early detection and prevention of ovarian cancer are potentially profound. The clinical uses of karyometric analysis of risk include (*a*) quantitation of risk using a more robust measurement than family history, (*b*) as a screening tool when karyometry is more automated, and (*c*) as a surrogate biological end point in ovarian cancer chemoprevention trials.

References

1. Greene MH, Clark JW, Blayney DW. The epidemiology of ovarian cancer. Semi Oncol 1984;11:209–26.
2. Easton DF, Ford D, Bishop DT. Breast and ovarian cancer incidence in *BRCA-1* mutation carriers. Am J Hum Genet 1995;56:265–71.

3. Deligdisch L, Miranda C, Barba J, Gil J. Ovarian dysplasia: nuclear texture analysis. Cancer 1993;72:325–57.
4. Deligdisch L, Gil J, Kerner K, Wu HS, Beck D, Gershoni-Baruch R. Ovarian dysplasia in prophylactic oophorectomy specimens, cytogenetic and morphometric correlations. Cancer 1999;86:1544–50.
5. Salazar H, Godwin AK, Daly MB, et al. Microscopic benign and invasive malignant neoplasms and a cancer-prone phenotype in prophylactic oophorectomies. J Natl Cancer Inst 1996;88:1810–20.
6. Lu K, Garber J, Cramer D, et al. Occult ovarian tumors in women with *BRCA-1* or *BRCA-2* mutations undergoing prophylactic oophorectomy. J Clin Oncol 2000;18:2728–32.
7. Puls L, Powell D, DePriest PD, et al. Transition from benign to malignant epithelium in mucinous and serous ovarian cystadenocarcinoma. Gynecol Oncol 1992;47:53–7.
8. Stratton JF, Buckley CH, Lowe D, Ponder BAJ; UKCCCR Familial Ovarian Cancer Study Group. Comparison of prophylactic oophorectomy specimens from carriers and non-carriers of a *BRCA-1* or *BRCA-2* gene mutation. J Natl Cancer Inst 1999;91:626–8.
9. Barakat RR, Federici MG, Saigo PE, Robson ME, Offit K, Boyd J. Absence of premalignant histologic, molecular or cell biologic alterations in prophylactic oophorectomy specimens from *BRCA-1* heterozygotes. Cancer 2000; 89:383–90.
10. Narod SA, Dube MP, Klijn J, Lubinski J, Lynch HT, Ghadirian P. Oral contraceptives and the risk of breast cancer in *BRCA-1* and *BRCA-2* mutation carriers. J Natl Cancer Inst 2002;94:1773–9.
11. Bartels PH, Montironi R, Hamilton PW, Thompson D, Vaught L, Bartels HG. Nuclear chromatin texture in prostatic lesions. II. PIN and malignancy associated changes. Anal Quant Cytol Histol 1998;20:397–406.
12. Anderson N, Houston J, Kirk SJ, et al. Malignancy associated changes in lactiferous duct epithelium. Anal Quant Cytol Histol 2003;25:63–72.
13. Berry DA, Parmigiani G, Sanchez J, Schildkraut J, Winer E. Probability of carrying a mutation of breast-ovarian cancer gene *BRCA1* based on family history [see comment]. J Nat Cancer Inst 1997;89:227–38.
14. Young T, Verbeek, PW, Mayall B. Characterization of chromatin distributions in cell nuclei. Biometry 1968;7:467–74.
15. Galoway M. Texture analysis using gray level run lengths. Computer Graphs and Image Processing 1975;4:172.
16. Bartels PH, da Silva VD, Montironi R, et al. Chromatin texture signatures in nuclei from prostate lesions. Anal Quant Cytol Histol 1998;20:407–16.
17. Weyn B, Jacob W, da Silva VD, et al. Data representation and reduction for chromatin texture in nuclei from premalignant prostatic, esophageal and colonic lesions. Cytometry 2000;41:133–8.
18. Wied GL, Bartels PH, Bahr GF, Oldfield DG. Taxonomic intracellular analytic system (TICAS) for cell identification. Acta Cytol 1968;12:180–204.
19. Beal EMI. Euclidean cluster analysis. Bull Intl Stat Inst 1969;43:21–43.
20. Montironi R, Scarpelli M, Mazzucchelli R, et al. Sub-visual chromatin changes are detected in the histologically normal urothelium in patients with synchronous papillary carcinoma. Hum Pathol 2003;34:893–901.
21. Wied GL, Bartels PH, Bibbo M, Sychra JJ. Cytomorphometric markers for uterine cancer in intermediate cells. Anal Quant Cytol Histol 1980;2:257–63.
22. Susnik B, Worth A, LeRiche J, Palcic G. Malignancy associated changes in the breast. Changes in chromatin distribution in epithelial cells in normal appearing tissue adjacent to cancer. Anal Quant Cytol Histol 1995;17:62–8.
23. Montag AG, Bartels PH, Dytch HE, Lerma-Puertas E, Michelassi F, Bibbo M. Karyometric features in nuclei near colonic adenocarcinoma. Statistical analysis. Anal Quant Cytol Histol 1991;13:159–67.
24. Bibbo M, Bartels PH, Galera-Davidson H, Dytch HE, Wied GL. Markers for malignancy in the nuclear texture of histologically normal tissue from patients with thyroid tumors. Anal Quant Cytol Histol 1986;8:168–76.